

Dynamics of Fabry-Perot Resonators with Suspended Mirrors

I. Nonlinear Coupled Oscillators

M. Rakhmanov and A. Arodzero

*LIGO Project
California Institute of Technology
Pasadena, CA 91125*

Abstract

The dynamics of Fabry-Perot cavity with suspended mirrors is described. The suspended mirrors are nonlinear oscillators interacting with each other through the laser circulating in the cavity. The degrees of freedom decouple in normal coordinates, which are the position of the center of mass and the length of the cavity. We introduce two parameters and study how the dynamics changes with respect to these parameters. The first parameter specifies how strong the radiation pressure is. It determines whether the cavity is multistable or not. The second parameter is the control parameter, which determines location of the cavity equilibrium states. The equilibrium state shows hysteresis if the control parameter varies within a wide range. We analyze stability of the equilibrium states and identify the instability region. The instability is explained in terms of the effective potential: the stable states correspond to local minima of the effective potential and unstable states correspond to local maxima. The minima of the effective potential defines the resonant frequencies for the oscillations of the cavity length. We find the frequencies, and analyze how to tune them. Multistability of the cavity with a feedback control system is analyzed in terms of the servo potential. The results obtained in this paper are general and apply to all Fabry-Perot cavities with suspended mirrors.

Contents

1	Introduction	3
2	Dynamical Equations and Regimes	5
2.1	Mirror Coordinates	5
2.2	Equations for Field Dynamics	6
2.3	Forces Acting on Mirrors	7
2.4	Control Parameter	8
2.5	Equations of Motion for Mirrors	8
2.6	Dynamical Regimes	9
2.7	Self-consistent Field in Adiabatic Regime	10
3	Normal Coordinates	11
3.1	Forces due to Radiation Pressure	11
3.2	Normal Modes	12
3.3	Center of Mass and Observability	12
3.4	Cavity Length	13
4	Equilibrium States	14
4.1	Static Solutions	14
4.2	Strength of Radiation Pressure	14
4.3	Equilibrium Condition	15
4.4	Graphical Construction of Equilibrium States	16
4.5	Condition for Multistability	16
4.6	Higher order bifurcations	17
5	Stability and Hysteresis	18
5.1	Multistability of Fabry-Perot cavity	18
5.2	Hysteresis of Mirror Position	20
5.3	Boundaries of Instability	21
6	Hamiltonian Dynamics	22
6.1	Conditions for Adiabatic Motion	22
6.2	Effective Potential	22
6.3	Global Properties of Effective Potential	23
6.4	Minima and Maxima of the Effective Potential	24
7	Resonance of Cavity Length	25
7.1	Resonant Frequency	25
7.2	Adjustment of Resonance Frequencies	26
7.3	Plateaus of the Effective Potential	27
7.4	Period of Anharmonic Oscillations	28

8 Implications for Control System	29
8.1 Pound-Drever Locking Servo	29
8.2 Multistability in Presence of Servo	29
8.3 Equilibrium and DC-bias	30
8.4 Stability Provided by Servo	31
9 Conclusions	32
A Parameters of LIGO Fabry-Perot Cavities	35
B Derivation of Field Equations	36
C Some properties of Airy function	37

1 Introduction

Very long Fabry-Perot cavities serve as measuring devices for interferometric gravitational wave detectors. Several such detectors are currently under construction [1, 2, 3]. The cavities are planned to have high circulating power and large storage time. For example, LIGO (Laser Interferometer Gravitational wave Observatory) Fabry-Perot cavities will accumulate 10 kW of power and will have roughly 1 ms of storage time.

The suspended mirrors are designed to move freely along the direction of the beam propagation. Due to multi-beam interference in the Fabry-Perot cavity the motion of the mirrors strongly affects the light inside the cavity. The light, in turn, affects the motion of the mirrors by exerting radiation pressure on them. The interaction of light in the cavity with the suspended mirrors through radiation pressure gives rise to a nonlinear dynamics. Finite time of light propagation in the cavity introduces a time delay in the dynamics. The propagation time gives rise to storage time. Thus a Fabry-Perot cavity is a dynamical system with delay; such systems are known to have instabilities [4].

The significance of the “spring” action and the “damping” effect of the radiation pressure for the dynamics of the Fabry-Perot cavity was pointed out by Braginskii [5]. The cavity with one suspended mirror driven by radiation pressure was studied experimentally by Dorsel et al [6, 7, 8, 9]. The main results reported in these papers are observations of optical bistability and mirror oscillations with frequencies determined by the radiation pressure. These authors analyzed their results using the adiabatic approximation for the intra-cavity field. At about the same time Deruelle and Tourrenc studied the Fabry-Perot cavity with suspended mirrors theoretically [10, 11]. Their analysis revealed delay-induced instability caused by the radiation pressure in the cavity. This instability was further studied by other researchers [12, 13]. Stabilization of the Fabry-Perot cavity by a control system was discussed by Meers and MacDonald [14]. Recently, the radiation pressure induced dynamics of Fabry-Perot cavities attracted attention of the VIRGO group in connection with the design of the length control system of their detector [15]. Similar research has been done in LIGO and is presented in this paper.

Emerging laser gravitational wave detectors require detailed modeling and pose new questions for the study of dynamics. From a phenomenological point of view, there is a question of what are the parameters that define the universal properties of Fabry-Perot cavities with suspended mirrors, and how the dynamics changes with respect to these parameters. From a point of view of applications, there is a question of how to generalize the results obtained in table-top experiments to large scale Fabry-Perot cavities of the gravitational wave detectors.

In this paper we attempt to provide a phenomenology of the Fabry-Perot cavities for modeling and optimization of the performance of LIGO interferometers. Due to the complexity of the subject we split the discussion into two papers. In the first paper we study various aspects of the nonlinearity in the dynamics, leaving aside the time delay instabilities. In the second paper [16] we consider the time delay instabilities and study the dynamics of a Fabry-Perot cavity with a realistic control system.

In this paper we formulate the dynamics in terms of normal coordinates: the cavity length and the cavity center of mass. We show that a small part of the radiation pressure in the cavity, the excess force, excites the cavity center of mass. In absence of the excess radiation pressure, the dynamics of the cavity length is equivalent to the dynamics of a suspended mirror in a cavity, which has one mirror suspended and one mirror fixed. To study the universal properties of the cavity dynamics,

such as multistability, we introduce two parameters. The first parameter is a control parameter which allows us to select the equilibrium state. The second parameter characterizes strength of the radiation pressure and determines whether the system is stable or multistable and how many equilibrium states are there. The results obtained in this paper are general and apply to any Fabry-Perot cavity with suspended mirrors. Numerical calculations and modeling with parameters of LIGO cavities are given throughout this paper.

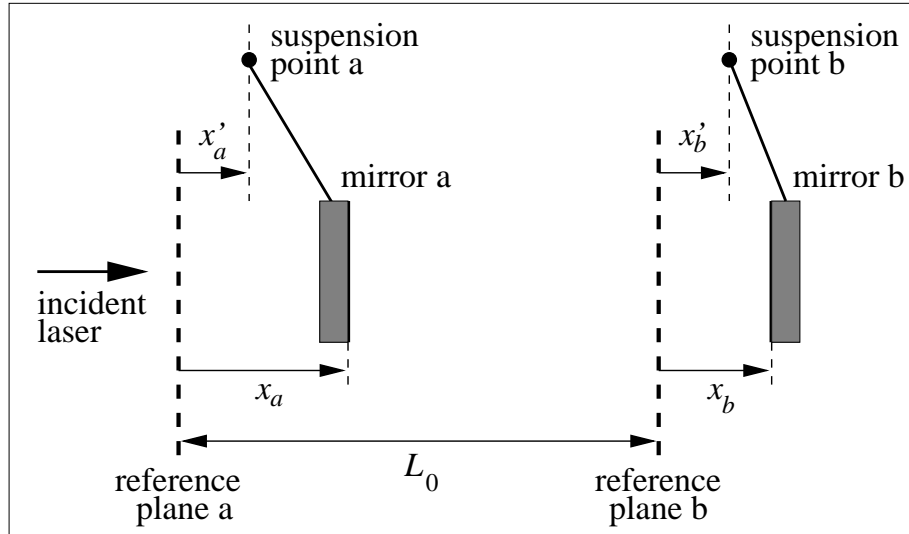
The paper is organized as follows. In Section 2 we describe the equations of motion and define the control parameter. In Section 3 we formulate the dynamics in normal coordinates. In Section 4 we construct equilibrium states and introduce the specific radiation pressure. In Section 5 hysteresis and instabilities are described. In Section 6 the global properties of the dynamics are analyzed in terms of the effective potential. In Section 7 we provide explicit formulas and numerical values for the cavity resonant frequencies. In Section 8 we briefly describe nonlinear dynamics of the cavity with a control system.

2 Dynamical Equations and Regimes

2.1 Mirror Coordinates

The dynamical system we study in this paper is a Fabry-Perot cavity with two suspended mirrors, labeled by a and b , and a laser incident on the cavity from one side. A suspended mirror is a rigid body with six degrees of freedom, whose dynamics depends on the suspension design. In this paper we neglect angular degrees of freedom of the mirrors and consider only the motion of their center of mass. We also neglect the side motion of the mirrors. In this approximation the mirrors are always aligned to the incident beam and move parallel to themselves as simple pendula. We specify the mirror positions by their coordinates, $x_a(t)$ and $x_b(t)$, in the inertial coordinate frames as shown on figure 1. The mirror suspension points are also moving, their coordinates are $x'_a(t)$ and $x'_b(t)$.

Figure 1: Coordinates of mirrors and their suspension points



The two inertial coordinate frames are separated by a large distance, the nominal cavity length, L_0 , which we consider fixed. The actual length of the cavity depends on mirror positions in their respective coordinate frames:

$$L = L_0 + x_b(t) - x_a(t). \quad (1)$$

The large cavity length of the gravitational wave detectors makes the delay time,

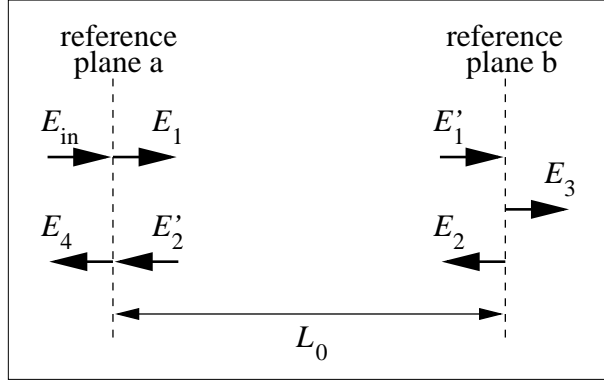
$$T = \frac{L_0}{c}, \quad (2)$$

to be non-negligible. For example, in LIGO interferometers the cavities are 4km long and the corresponding delay time is roughly $13 \mu\text{s}$.

2.2 Equations for Field Dynamics

Multibeam interference of laser in long Fabry-Perot cavities of gravitational wave detectors is far more complex than a similar process in short Fabry-Perot interferometers with fixed length which are commonly used for laser spectroscopy. Both the motion of suspended mirrors and the delay times affect the interference and give rise to a complex dynamics. We describe dynamics of the laser in the cavity in terms of complex amplitudes of the electric field. These complex amplitudes correspond to the traveling electro-magnetic waves and are defined at some locations. Usually the amplitudes are defined at the mirror surfaces. However, the suspended mirrors are moving and such a choice would require account for Doppler effects. Instead, we define the amplitudes at the reference planes which are fixed in the inertial coordinate frames.

Figure 2: Notations for fields and reference planes



Our notations for the amplitudes of the electro-magnetic waves are shown in Fig. 2. The amplitude of the wave, incident on the front mirror, is E_{in} . The amplitudes of the forward-propagating wave inside the cavity, defined at the two reference planes, are E_1 and E'_1 . Similarly, the amplitudes of the backward-propagating wave are E_2 and E'_2 . The amplitudes of the cavity transmitted and reflected waves are E_3 and E_4 .

Propagation of the laser inside the cavity is described by the delay equations:

$$E'_1(t) = E_1(t - T), \quad (3)$$

$$E'_2(t) = E_2(t - T). \quad (4)$$

These and other equations for the complex amplitudes are derived in the Appendix B. The equations for reflection and transmission of the laser at the end mirror are:

$$E_2(t) = -r_b e^{-2ikx_b(t)} E'_1(t), \quad (5)$$

$$E_3(t) = t_b E'_1(t), \quad (6)$$

where r_b is the reflectivity and t_b is the transmissivity of the end mirror.

Using the superposition principle we obtain similar equations for the front mirror:

$$E_1(t) = t_a E_{in} - r_a e^{2ikx_a(t)} E'_2(t), \quad (7)$$

$$E_4(t) = t_a E'_2(t) + r_a e^{-2ikx_a(t)} E_{in}, \quad (8)$$

where r_a and t_a is the reflectivity and the transmissivity of the front mirror. Numerical values for the reflectivities and the transmissivities of the mirrors in LIGO cavities are given in the Appendix A.

The equations (3-8) describe dynamics of the laser interacting with the moving mirrors of the cavity. These equations can be reduced to one equation with one field, which is called the self-consistent field. All other fields can be expressed in terms of the self-consistent field through the field equations above.

We choose the forward-propagating field to be the self-consistent field. Let the amplitude of the self-consistent field be $E(t)$ (same as $E_1(t)$). Then the equation for dynamics of the self-consistent field is

$$E(t) = t_a E_{in} + r_a r_b e^{-2ikz(t)} E(t - 2T), \quad (9)$$

where $z(t)$ is the relative mirror position defined as

$$z(t) = x_b(t - T) - x_a(t). \quad (10)$$

The quantity, $L_0 + z(t)$, is the distance between the mirrors in relativistic sense.

Since the speed of light is finite we cannot obtain information about the instantaneous cavity length defined in eq. (1). However, we can measure the relativistic cavity length, $z(t)$, by observation of one of the cavity fields. This can be done using the Pound-Drever signal extraction scheme. The Pound-Drever signal is based on observation of the cavity reflected laser

$$V_{P-D} \sim \text{Im}\{e^{2ikx_a(t)} E_4(t)\} \quad (11)$$

$$\sim \text{Im}\{E(t)\}, \quad (12)$$

which is defined in terms of the self-consistent field and, therefore, depends on the cavity length, $z(t)$.

In the expression, eq. (10), the delay appears in the coordinate of the end and not the front mirror. This is because upon entering the cavity the laser first reflects off the end mirror and then reflects off the front mirror.

2.3 Forces Acting on Mirrors

Dynamics of the suspended mirrors is defined by the forces acting on them. Since we analyze only longitudinal motion of the mirrors we consider only horizontal components of the forces. The horizontal component of the wire tension, acting on the front mirror, is

$$-m_a \omega_0^2 (x_a - x'_a), \quad (13)$$

where m_a is the mass of the front mirror and ω_0 is the pendulum frequency. There is a similar expression for the end mirror.

The laser circulating in the cavity and the incident laser exert pressure on the mirrors. Let the radiation pressure on the front and the end mirror be R_a and R_b . These forces are defined by the amplitudes of the fields as follows:

$$R_a = \frac{1}{c} \left\{ |E_{in}|^2 - |E_1|^2 - |E'_2|^2 + |E_4|^2 \right\}, \quad (14)$$

$$R_b = \frac{1}{c} \left\{ |E'_1|^2 + |E_2|^2 - |E_3|^2 \right\}. \quad (15)$$

Many control schemes, including the control system of LIGO arm cavities, require actuators on the mirrors. The actuators can be coil-magnet pairs, electro-static boards or other devices. For our analysis the details of the actuators are not important. We only assume that actuators are perfectly aligned and apply forces to the mirrors in the direction of the beam propagation. Let the actuator forces be F_a^{act} and F_b^{act} .

There is also a friction force due to energy losses in the suspension wires and the actuators. We assume that the friction is proportional to velocity. Then the friction force acting on the front mirror can be written as

$$-m_a\gamma\dot{x}_a, \quad (16)$$

where γ is the damping coefficient. A similar expression can be obtained for the end mirror. Typically the damping coefficient is very small: $\gamma/\omega_0 \sim 10^{-5}$.

Numerical values for the parameters of LIGO interferometers are given in Appendix A.

2.4 Control Parameter

Let us consider the sum of the pendulum restoring force and the actuator force for the front mirror:

$$-m_a\omega_0^2(x_a - x'_a) + F_a^{\text{act}}. \quad (17)$$

There are two parameters here: the position of the suspension point and the actuator force. The mirror can be controlled through both the actuator and the suspension point. However, the dynamics depends only on the sum of the two parameters, and not separately on each one. Therefore, we combine the two parameters into a new parameter

$$u_a = x'_a + \frac{F_a^{\text{act}}}{m_a\omega_0^2}. \quad (18)$$

This is the control parameter for the front mirror. A similar parameter, u_b , can be introduced for the end mirror.

The control parameter has dimension of length and the meaning of an equivalent displacement of the suspension point. The equivalence is based on the conversion factor $(m\omega_0^2)^{-1}$, which for LIGO is roughly 4.2 millimeter per newton of the actuator force.

Moving the suspended mirrors at high frequencies is easier using the actuator. However, applying large displacements to the mirror at low frequencies is better through the suspension point. Therefore in a realistic control system the control parameter, u , may obtain its high frequency component from the actuator force and its low frequency component from the position of the suspension point.

2.5 Equations of Motion for Mirrors

The equations of motion for the mirrors are

$$\ddot{x}_a + \gamma\dot{x}_a + \omega_0^2x_a = \omega_0^2u_a + \frac{R_a}{m_a}, \quad (19)$$

$$\ddot{x}_b + \gamma\dot{x}_b + \omega_0^2x_b = \omega_0^2u_b + \frac{R_b}{m_b}. \quad (20)$$

These are the equations for a pair of damped harmonic oscillators driven by forces of the radiation pressure. The oscillators are not independent: they are interacting with each other through the laser which acts as a spring connecting the mirrors. The “spring” is nonlinear and has time delay.

2.6 Dynamical Regimes

A Fabry-Perot cavity has two intrinsic time scales: one is the delay time, T , the other is the storage time

$$\tau = \frac{2T}{|\ln(r_a r_b)|}. \quad (21)$$

Correspondingly, there are two intrinsic frequencies defined by the cavity: the free spectral range ($f_{\text{FSR}} = (2T)^{-1}$) and the cavity low pass frequency

$$f_{\text{cav}} = \frac{1}{2\pi\tau}. \quad (22)$$

Therefore, there are three dynamical regimes for the Fabry-Perot cavity.

Let δt be a characteristic time for a dynamic process involving changes in the mirror positions and fields. Let f be the characteristic frequencies of the process. The three regimes are:

1. decoupled regime: $\delta t \ll T$ ($f \gg f_{\text{FSR}}$),
2. delay regime: $T \ll \delta t \ll \tau$ ($f_{\text{cav}} \ll f \ll f_{\text{FSR}}$),
3. adiabatic regime: $\delta t \gg \tau$ ($f \gg f_{\text{cav}}$).

The first regime corresponds to very fast changes in mirror positions and fields in the Fabry-Perot cavity. The decoupled regime can be understood on the following example. First the mirrors are at rest. Then one mirror acquires some velocity, changes its position and stops. If the entire process takes time less than T the second mirror becomes affected by the process after the first mirror comes to rest. Therefore, during such process the mirrors are independent of each other. This is nothing but a relativistic causality limit. In LIGO interferometers the processes with frequencies above 37.5 kHz belong to the decoupled regime.

The second regime takes place when the changes in the mirror position are faster than transient processes in the cavity but not fast enough to decouple the mirrors. In this regime the transients caused by the mirror motion never die and the cavity never reaches equilibrium. In such a regime the motion of one mirror is constantly affected by the other mirror and the delays play crucial role. Dynamic processes in LIGO cavities with frequencies between 100 Hz and 10 kHz belong to this regime.

The third regime takes place when the mirrors move so slow that the laser transients can be neglected. In this case we can think of the laser circulating in the cavity as being in equilibrium with the mirrors. This is the adiabatic regime. In this regime the delays are not important. The adiabatic regime takes place in LIGO cavities at frequencies less than 100 Hz.

2.7 Self-consistent Field in Adiabatic Regime

In the adiabatic regime the mirror motion is so slow that we can neglect the delay time in the equation for the self-consistent field eq. (9) and obtain a solution:

$$E(t) = \frac{t_a E_{in}}{1 - r_a r_b e^{-2ikz(t)}}. \quad (23)$$

The value of the field in the adiabatic regime is completely defined by the current value of the cavity length, $z(t)$. The power in the cavity, which we define as the momentum carried by the forward-propagating wave ($P = |E|^2$) is also a function of the cavity length. The maximum power, P_{max} , depends on the mirror parameters and defines the cavity gain:

$$G_{cav} \equiv \frac{P_{max}}{P_{in}} = \frac{t_a^2}{(1 - r_a r_b)^2}. \quad (24)$$

The power as a function of length is described by the Airy formula

$$P = \frac{P_{max}}{1 + F \sin^2 k z(t)}, \quad (25)$$

also known as Airy intensity profile (see [17]). The constant, F , is the coefficient of finesse

$$F = \frac{4r_a r_b}{(1 - r_a r_b)^2}. \quad (26)$$

The relation between the parameter, F , and the finesse of Fabry-Perot cavity is given in Appendix C.

3 Normal Coordinates

3.1 Forces due to Radiation Pressure

The suspended mirrors are interacting with each other through the laser in the cavity. Therefore, the degrees of freedom which correspond to the mirrors are coupled. However, we can formulate the dynamics in terms of new degrees of freedom which are largely independent of each other. These new degrees of freedom are similar to the normal coordinates usually appeared in theory of coupled linear oscillators. Before we formulate the dynamics in terms of the normal coordinates we reduce the number of fields entering the general expressions for the radiation pressure on the mirrors, equations (14-15).

The radiation pressure on the end mirror, eq. (15) can be expressed entirely in terms of the self-consistent field:

$$R_b(t) = \frac{1}{c}(1 + r_b^2 - t_b^2)|E(t - T)|^2. \quad (27)$$

The radiation pressure on the front mirror is produced by the laser circulating in the cavity and the laser incident on the cavity, eq. (14). A constant flux of the incident laser produces constant radiation pressure on the front mirror:

$$R_{in} = \frac{1}{c}(1 + r_a^2 - t_a^2)|E_{in}|^2. \quad (28)$$

Therefore, we can write the radiation pressure on the front mirror as the sum:

$$R_a(t) = -R_b(t - T) + R_{in} + \Delta R(t). \quad (29)$$

In this equation the first term implies that the same force which is pushing the end mirror now will be pushing the front mirror in the opposite direction after time T . The second term is proportional to the power of the incident laser and accounts for the constant radiation pressure from outside the cavity. The last term, $\Delta R(t)$, which can be called the excess radiation pressure, accounts for the asymmetry between the mirrors and the interference between the incident laser and the laser circulating in the cavity. The excess force can also be expressed entirely in terms of the self-consistent field and the cavity length:

$$\Delta R(t) = \frac{\alpha}{c}|E(t - 2T)|^2 - \frac{4}{c}t_a r_a r_b \operatorname{Re}\{e^{-2ikz(t)} E_{in}^* E(t - 2T)\}, \quad (30)$$

where $\alpha = 1 - t_b^2 - r_b^2(r_a^2 - t_a^2)$, and the asterisk stands for complex conjugation.

In the adiabatic regime the excess force can be written explicitly as a function of length:

$$\Delta R = c^{-1} P_{max} \frac{\alpha + 4r_a r_b(r_a r_b - \cos 2kz)}{1 + F \sin^2 kz}. \quad (31)$$

Numerical estimates with LIGO parameters show that the excess radiation pressure, ΔR , is roughly four orders of magnitude less than the radiation pressure, R_b .

The constant radiation pressure, eq. (28), has no effect on the dynamics, but the excess force, eq. (30), makes the radiation pressure on the mirrors unbalanced and affects the dynamics.

3.2 Normal Modes

The normal coordinates are the position of the center of mass and the cavity length:

$$Z(t) = \frac{m_a x_a(t) + m_b x_b(t - T)}{m_a + m_b}, \quad (32)$$

$$z(t) = x_b(t - T) - x_a(t). \quad (33)$$

Note that both normal coordinates are affected by the delay due to the finite time of laser propagation in the cavity.

Similarly, we introduce the control parameters for the new coordinates:

$$U(t) = \frac{m_a u_a(t) + m_b u_b(t - T)}{m_a + m_b} + \frac{R_{in}}{c(m_a + m_b)\omega_0^2}, \quad (34)$$

$$u(t) = u_b(t - T) - u_a(t) - \frac{R_{in}}{cm_a\omega_0^2}. \quad (35)$$

To make the subsequent formulas simpler we hid the constant radiation pressure into the new control parameters. Also we define the reduced mass in a usual way:

$$\mu = \frac{m_a m_b}{m_a + m_b}. \quad (36)$$

In normal coordinates the dynamical equations are the equation for the center of mass and the equation for the cavity length:

$$\ddot{Z} + \gamma \dot{Z} + \omega_0^2 Z = \omega_0^2 U + \frac{\Delta R}{m_a + m_b}, \quad (37)$$

$$\ddot{z} + \gamma \dot{z} + \omega_0^2 z = \omega_0^2 u + \frac{R_b}{\mu} - \frac{\Delta R}{m_a}. \quad (38)$$

We see that the radiation pressure mostly affects one degree of freedom: the cavity length, $z(t)$. This is because the pressure on the front mirror is roughly equal and opposite to the pressure on the end mirror if we neglect the constant pressure from outside. The motion of the center of mass is affected by the radiation pressure only through the excess force.

3.3 Center of Mass and Observability

Dynamics of the center of mass of free cavity is defined exclusively by the excess radiation pressure, which, in turn, is defined by the cavity length, $z(t)$. As a result, changes in the cavity length excite motion of the center of mass. On the contrary, arbitrary motion of center of mass has no effect on the cavity length. Therefore we can ignore the dynamics of the center of mass and focus on the cavity length. However, few important points must be taken into account before we abandon the motion of the center of mass.

Although small motion of the center of mass ($\sim 1\mu\text{m}$) has no effect on the detector performance, large motion (~ 0.1 mm) will cause variations of the actuator gains. Therefore, the motion of the

cavity center of mass must be suppressed to the extent defined by the actuator's range. In particular, we must avoid exciting the motion of the center of mass by a control system. In gravitational wave detectors the control system suppresses motion of the mirror under seismic disturbances by applying forces to the mirrors through the actuators. Therefore the control system can excite the motion of the center of mass, unless the control signals are synchronized:

$$\delta u_a(t) = -\frac{m_b}{m_a} \delta u_b(t - T). \quad (39)$$

Unlike the cavity length the center of mass is not observable in a strict relativistic sense. To obtain information about the cavity's center of mass requires setting up an inertial frame, which is impossible for the ground based gravitational wave detectors. This poses a problem of observability for control of the Fabry-Perot cavity, which can be stated as follows. The cavity length is known with high precision (better than 10^{-13}m) but the center of mass can only be measured approximately (up to $1\mu\text{m}$). Therefore the cavity length can only be controlled approximately. Since the two degrees of freedom are largely independent poor observability and control of the center of mass do not affect the dynamics of the cavity length. Therefore, as long as the motion of the center of mass remains small, it can be ignored.

3.4 Cavity Length

The degree of freedom most important for understanding the response of Fabry-Perot cavity as a part of the gravitational wave detector is the cavity length $z(t)$.

In the following discussion of the cavity length dynamics we neglect the excess radiation pressure, ΔR . To simplify following formulas we make the approximation: $1 + r_b^2 - t_b^2 \approx 2$ in the eq. 27 and write the radiation pressure on the end mirror as

$$R_b(t) = \frac{2}{c} |E(t - T)|^2. \quad (40)$$

This is a good approximation for high reflective mirrors, such as the end mirrors of LIGO cavities.

The dynamics of the cavity length is independent of the dynamics of the center of mass and can be studied separately. The equations for the cavity length dynamics include only the cavity length and the self-consistent field:

$$\ddot{z} + \gamma \dot{z} + \omega_0^2 z = \omega_0^2 u + \frac{2}{c\mu} |E(t - 2T)|^2, \quad (41)$$

$$E(t) = t_a E_{in} + r_a r_b e^{-2ikz(t)} E(t - 2T), \quad (42)$$

The iteration equation (42) allows us to calculate the amplitude $E(t)$ at discrete times. The time step is the cavity round-trip time, $2T$. The value of the amplitude between the steps can be found by delaying its value at the last iteration.

These equations are equivalent to the equations of the dynamics of the Fabry-Perot cavity with front mirror fixed and the end mirror suspended from wires, provided the mass of the end mirror is equal to the reduced mass.

4 Equilibrium States

4.1 Static Solutions

Equilibrium states of the cavity are static solutions of the equations (41) and (42). For static states these equations simplify and can be written as

$$\mu\omega_0^2(z - u) = \frac{2}{c} |E|^2, \quad (43)$$

$$E = \frac{t_a E_{in}}{1 - r_a r_b e^{-2ikz}}. \quad (44)$$

The complex field, E , can be eliminated from the equations (43) and (44) and the equilibrium condition can be written entirely in terms of the cavity length:

$$\mu\omega_0^2(z - u) = \frac{R_{max}}{1 + F \sin^2 kz}. \quad (45)$$

Here R_{max} is the maximum radiation pressure on the end mirror which corresponds to the maximum power in the cavity:

$$R_{max} = \frac{2}{c} P_{max}. \quad (46)$$

The equation (45) shows that in equilibrium the radiation pressure is balanced by the pendulum restoring force.

Numerical values of the power and the radiation pressure in LIGO Fabry-Perot cavities are given in the Table 1.

Table 1: Power and radiation pressure in LIGO Fabry-Perot cavities

	$P_{in}(W)$	$P_{max}(W)$	$F_{max}(N)$
40m LIGO Prototype	0.25	160	1.1×10^{-6}
4km LIGO	90	12000	7.8×10^{-5}

4.2 Strength of Radiation Pressure

To characterize strength of the radiation pressure we introduce a dimensionless parameter

$$\sigma = \frac{kR_{max}}{\mu\omega_0^2}, \quad (47)$$

where $k = 2\pi/\lambda$ is the wave number, μ is the reduced mass and ω_0 is the pendulum frequency. The parameter σ shows how strong the radiation pressure is compared to the pendulum restoring force.

This parameter allows us to characterize nonlinearities induced by the radiation pressure quantitatively. As a measure of nonlinearities, the parameter σ is similar to the Reynolds number in fluid dynamics.

The parameter σ also allows us to establish equivalence of the equilibrium states of different Fabry-Perot cavities. Namely, the equilibrium states of a Fabry-Perot cavity with high circulating power and heavy mirrors are equivalent to those of a cavity with low power and light mirrors if the two cavities have the same σ .

The parameter σ has a simple geometric interpretation. From the equilibrium condition, eq. (45), we see that the maximum increase in the cavity length due to radiation pressure is σ/k . Therefore, σ/π is the maximum number of fringes the mirrors can be pushed apart by the radiation pressure.

We can think of σ as a function of the incident power

$$\sigma = \frac{2kG_{cav}}{c\mu\omega_0^2} P_{in}, \quad (48)$$

where G_{cav} is the cavity gain, eq. (24). Therefore, the simplest way to change the parameter σ is to vary the input power of the Fabry-Perot cavity.

4.3 Equilibrium Condition

The equilibrium states depend on properties of Airy function:

$$A(\phi) = \frac{1}{1 + F \sin^2 \phi}. \quad (49)$$

A discussion of Airy function can be found in ref. [17]. Some of the properties of Airy function are given in the Appendix C.

Let us introduce the phase variables for the cavity length and the control parameter:

$$\phi = kz, \quad (50)$$

$$\eta = ku. \quad (51)$$

In terms of the phase variables the condition for equilibrium, eq. (45), becomes

$$\frac{1}{\sigma}(\phi - \eta) = A(\phi). \quad (52)$$

By solving this equation we can find equilibrium states, ϕ , for any given value of the control parameter, η . Even more important is an inverse application of the equilibrium condition. Namely, we can turn any state, ϕ , into an equilibrium state by adjusting the control parameter, η , according to

$$\eta = \phi - \sigma A(\phi). \quad (53)$$

An operation point for the Fabry-Perot cavity is an equilibrium state, at which we want to maintain the cavity. We select the operation point by specifying the phase, ϕ_0 , and by adjusting the control parameter according to the eq. (53).

In LIGO interferometers the operation point is chosen at the maximum of Airy function ($\phi_0 = \pi n$), where n is integer. To obtain an equilibrium state at these points we must have the control parameter set to the following values

$$u = \frac{\lambda}{2} \left(n - \frac{\sigma}{\pi} \right). \quad (54)$$

Since all the peaks of Airy function are equivalent the different values of the control parameter, which correspond to different values of n , are all equivalent. The least absolute value of the control parameter corresponds to $n = \text{round}(\sigma/\pi)$. Since the control parameter is a linear combination of the actuator force and the displacement of the suspension point, eq.(18), this condition can be achieved in two ways. We can either apply the forces to the mirrors or shift the suspension points. The larger the actuator forces the higher the noise in the actuators. Therefore, it is desirable to operate the cavities with as less force on the mirrors as possible.

4.4 Graphical Construction of Equilibrium States

The equilibrium states are given by the nonlinear equation, eq. (52), which cannot be solved analytically. However, we can analyze the equilibrium states using a graphical construction. The graphical method for finding the equilibrium states appears in several papers, for example, in ref. [18]. In our approach we use the graphical method not only to show approximate locations of the equilibrium states but also to derive exact statements about equilibrium and stability of the Fabry-Perot cavity.

The graphical construction is to plot the functions in the left and the right sides of the equation (52) and look for their intersections. The left side of the equation is the pendulum restoring force in dimensionless units. It corresponds to a straight line shown in Fig. 3. The line has the slope σ^{-1} and the intercept η . The right side of the equation is the Airy function, which is the radiation pressure normalized to unity at its maximum. The points, where the straight line intersects the Airy function, are the equilibrium states. In Figure 3 there are three equilibrium states: ϕ_1, ϕ_2 and ϕ_3 .

4.5 Condition for Multistability

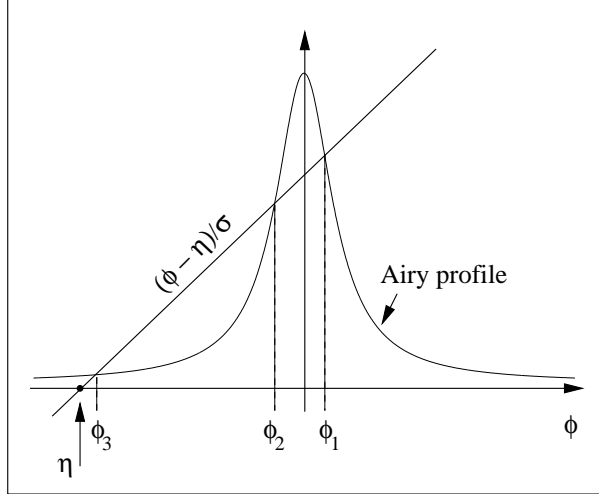
A Fabry-Perot cavity is multistable if it has more than one equilibrium state, which belong to the same value of the control parameter. To derive a condition for multistability consider a line tangential to the Airy profile at some point, ϕ_0 . The slope of the tangent line is $A'(\phi_0)$, the derivative of Airy function at this point. The highest slope of the tangent line corresponds to the maximum value of the derivative

$$\max\{A'\} \approx \frac{3}{8}\sqrt{3F}, \quad (55)$$

which is derived in Appendix C. If the slope of the straight line, which represents the pendulum restoring force, is greater than the maximum slope, the line intersects the Airy profile at only one point. Otherwise, the straight line and Airy profile can have several common points. Therefore, there is a critical value of the parameter σ , for which a qualitative change in the equilibrium states occurs. This critical value is defined by the maximum slope

$$\sigma_{cr} \equiv \frac{1}{\max\{A'\}} \approx \frac{8}{3\sqrt{3F}}, \quad (56)$$

Figure 3: Graphical Construction of Equilibrium States



and depends only on the finesse of the Fabry-Perot cavity. These geometric arguments lead us to the condition for multistability. The Fabry-Perot cavity is

$$\begin{aligned} \text{stable, if } & \sigma < \sigma_{cr} \\ \text{multistable, if } & \sigma > \sigma_{cr}. \end{aligned}$$

LIGO Fabry-Perot cavities are multistable: $\sigma = 3.9$, which is greater than the critical value, $\sigma_{cr} = 0.012$.

4.6 Higher order bifurcations

At low radiation pressure ($\sigma < \sigma_{cr}$) the cavity has only one equilibrium state. If we increase the radiation pressure and reach the critical point ($\sigma = \sigma_{cr}$) the equilibrium state splits into three states, as shown in Fig. 4. Two of the new states are stable and one is unstable. Such a phenomenon is common in nonlinear physics and is called the pitchfork bifurcation [19], [20].

If we keep increasing the radiation pressure, at some point another bifurcation occurs and more equilibrium states are created. We can continue the process and obtain an infinite number of bifurcations in the Fabry-Perot cavity. The values of the parameter σ , at which these bifurcations occur, can be found from the graphical construction shown in Fig. 5. These values are $\sigma_n \approx \pi n$ where $n = 1, 2, \dots$ is the order of the bifurcation. In terms of power the condition for the n th order bifurcation to occur is

$$P_{max} = \frac{1}{4} c \mu \omega_0^2 \lambda n. \quad (57)$$

Exact number of equilibrium states depends not only on the parameter σ , but also on the control parameter, u .

Figure 4: Pitchfork bifurcation

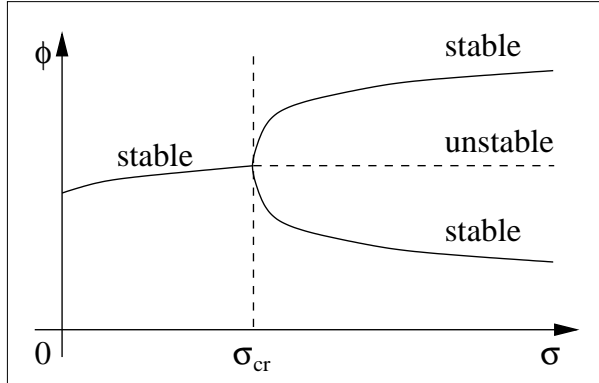
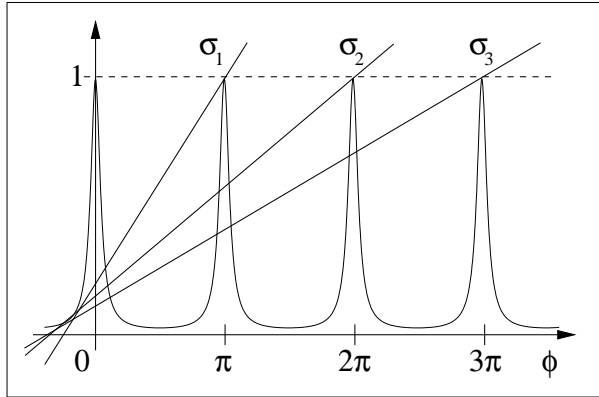


Figure 5: Higher order bifurcations



5 Stability and Hysteresis

5.1 Multistability of Fabry-Perot cavity

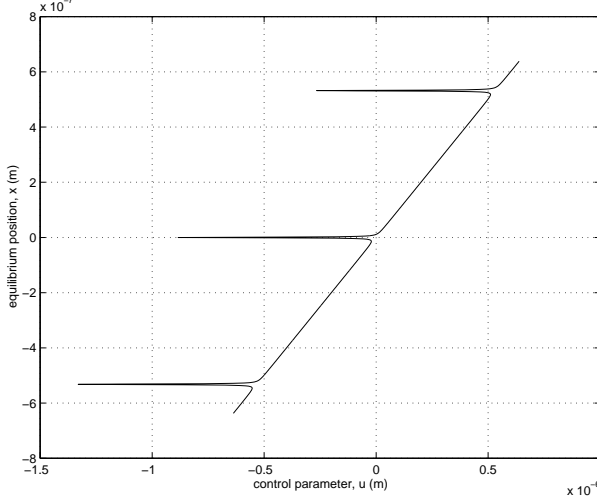
Fabry-Perot cavity with suspended mirrors is a multistable dynamical system. There are multiple equilibrium states in the cavity which correspond to the same value of the control parameter. Some of them are stable and some are unstable. A multistable cavity being brought near unstable equilibrium state moves to a nearest stable equilibrium state, which belongs to the same value of the control parameter.

Multistability of the Fabry-Perot cavity manifests itself in multi-valued functions describing the cavity state. For example, the equilibrium cavity length, z , is a multi-valued function of the control parameter, u . This function is defined implicitly:

$$z = u + \frac{\sigma}{k} A(kz), \quad (58)$$

and is shown on Fig. 6.

Figure 6: Multistability of cavity length



A similar multistable response appears if we vary the input power, P_{in} , within a wide range, but keep the control parameter fixed. This way we obtain the power in the cavity, P , as a multi-valued function of the input power. Such function also is defined implicitly:

$$P = \frac{G_{cav} P_{in}}{1 + F \sin^2 \left(ku + \frac{2kP}{c\mu\omega_0^2} \right)}. \quad (59)$$

The plot of this function for a particular value of the control parameter ($u = -\frac{2P_{max}}{c\mu\omega_0^2}$) is shown in Fig. 7. This is a typical multistability curve similar to those, which frequently appear in studies of the bistable optical devices [21], [22].

Both plots above have retrograde segments which correspond to unstable equilibrium states of the cavity. In general any state on a retrograde part of a multistable curve is unstable [20].

The formula which describes the power inside the cavity as a function of the input power, eq. (59), is equivalent to the corresponding formula for the fixed length cavity filled with a non-linear medium. The index of refraction of such medium has a quadratic nonlinearity

$$n(E) = n_0 + n_2 |E|^2, \quad (60)$$

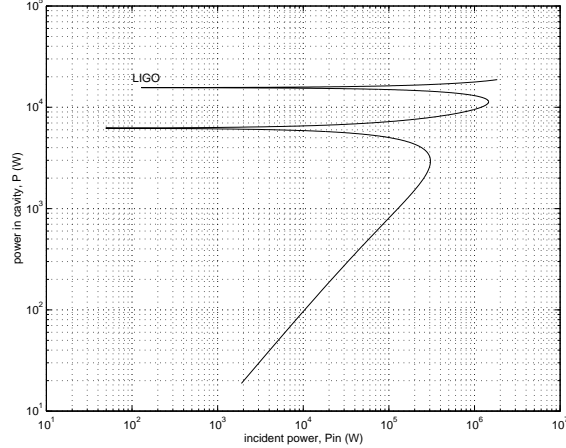
where n_0 and n_2 are the coefficients of the nonlinear index of refraction. A review of the extensive research which had been done on the cavities with the quadratic nonlinearity can be found in [21]. Here we obtain an exact condition for this equivalence. In the equation (59) the phase is a function of the power:

$$\phi = ku + \frac{2k}{c\mu\omega_0^2} |E|^2. \quad (61)$$

A similar dependence appears in the cavity with fixed length but filled with the nonlinear medium. The equivalence is achieved by tuning the parameters according to the equation:

$$n_2 l_0 = \frac{2k}{c\mu\omega_0^2}, \quad (62)$$

Figure 7: Multistability of power in Fabry-Perot cavity. The parameters are chosen so that the curve goes through the LIGO operation point



where l_0 is the length of the cavity with the nonlinear medium. Therefore, equilibrium states of a cavity with suspended mirrors are equivalent to those of a cavity filled with the nonlinear medium if the condition, eq. (62) is satisfied. This equivalence allows us to extend some results obtained for the cavities with the medium to the cavity with suspended mirrors.

5.2 Hysteresis of Mirror Position

The instability causes jumps and a hysteresis to appear. In this section we describe the mirror jumps and the hysteresis in the mirror position in the Fabry-Perot cavity.

Assume that one mirror is at rest and the other is moving. Let this motion be so slow that the cavity remains in equilibrium. We can produce such motion by a slow change of the control parameter. The motion of the mirror is shown on the parameter-state diagram, Fig. 8.

Let “A” be a starting point. Assume that we force the mirror to move by changing the control parameter from u_A to u_B . As we increase the value of the control parameter the mirror moves steadily from point “A” through point H_1 to point H_2 . As the mirror reaches point H_2 a sudden transition to point H_3 occurs. This jump happens because both points H_2 and H_3 belong to the same value of the control parameter but point H_2 is unstable. After the mirror reaches point H_3 , it resumes its steady motion and reaches the point “B”. The sequence of states is

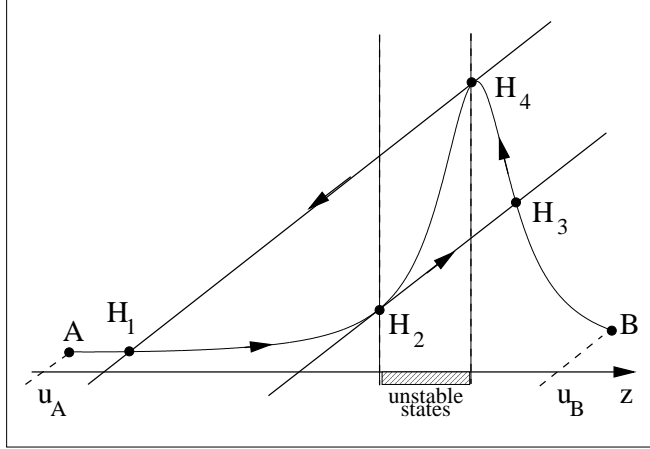
$$A \rightarrow H_1 \rightarrow H_2 \rightarrow H_3 \rightarrow B. \quad (63)$$

The jump $H_2 \rightarrow H_3$ is accompanied by a rapid build-up of power in the cavity, and, therefore, takes time of the order of the storage time to complete.

In the reverse process, we change the control parameter from u_B to u_A and thereby force the mirror to move in the opposite direction. On the way back the mirror does not retract its path. Instead, it follows a sequence

$$B \rightarrow H_3 \rightarrow H_4 \rightarrow H_1 \rightarrow A. \quad (64)$$

Figure 8: Hysteresis and instability region



The reverse motion of the mirror also has a jump but at a different place: point H_4 . The transition $H_4 \rightarrow H_1$ is accompanied by a rapid drop of power in the cavity. Thus a slow sweep of the mirror across the resonance is an irreversible process, known as hysteresis. The complete cycle:

$$H_1 \rightarrow H_2 \rightarrow H_3 \rightarrow H_4 \rightarrow H_1, \quad (65)$$

is the hysteresis loop, which is typical for nonlinear systems.

A similar hysteresis appears if we keep the control parameter fixed but vary the input power. Such hysteresis was observed by Dorsel and collaborators and is described in ref.[6].

5.3 Boundaries of Instability

The states on the retrograde segments of the multistability curve on Fig. 6 and Fig. 7 are unstable. These states form an instability region which is confined by the two tangent lines with the slope σ^{-1} , as shown in Fig. 8. The boundaries of the instability region are defined by the equation

$$A'(\phi) = \frac{1}{\sigma}. \quad (66)$$

There are two solutions of this equation, which are left and right boundaries of the instability region. In the large- F approximation the instability region is

$$-\left(\frac{2\sigma}{F}\right)^{\frac{1}{3}} < \phi_0 < -\frac{1}{2\sigma F}. \quad (67)$$

The left boundary corresponds to low power inside the Fabry-Perot cavity. The right boundary is located very close to the peak of the Airy function and corresponds to high power. For example, in the 4km LIGO interferometers the right boundary of the instability is $\phi_0 = -7.5\mu\text{rad}$. Thus the separation between the right boundary and the peak is very small, roughly a thousandth of the width of Airy function.

6 Hamiltonian Dynamics

6.1 Conditions for Adiabatic Motion

Motion of the mirrors belongs to the adiabatic regime only if it is slow; the characteristic time of such motion must be much greater than the cavity storage time. We define the characteristic time differently for small- and large-amplitude mirror motions.

We consider the amplitude small if it is less than the width of the resonance. Usually such motion is oscillatory. Then the characteristic time is equal to the period of these oscillations, T_{osc} . Therefore, the motion is adiabatic if $T_{\text{osc}} \gg \tau$.

Large-amplitude mirror motion takes place when the changes in the cavity length are greater than the width of resonance, x_w . During such motion the relative velocity of the mirrors, v , can be considered constant within the time the mirrors pass through a resonance. Then the characteristic time is the time it takes for the length to change by the width of one resonance: x_w/v . Therefore, the motion is adiabatic if $x_w/v \gg \tau$. This condition can also be seen as a requirement on the relative velocity of the mirrors. Namely, the large-amplitude mirror motion is adiabatic if $v \ll v_{ad}$, where v_{ad} is the adiabatic threshold velocity:

$$v_{ad} \equiv \frac{x_w}{\tau} \approx \frac{c\lambda}{\pi FL_0}. \quad (68)$$

The threshold velocity depends only on the parameters of the cavity and the wavelength of the laser. For LIGO Fabry-Perot cavities $v_{ad} = 7.4 \times 10^{-7}$ m/s.

6.2 Effective Potential

In the adiabatic regime the field inside the cavity, $E(t)$, is completely defined by the length, $z(t)$, see eq. (23). Therefore, we can eliminate the field and consider only the dynamics of the length. The equation for the length dynamics becomes

$$\ddot{z} + \gamma \dot{z} = -\omega_0^2(z - u) + \frac{1}{\mu} R_{\text{max}} A(kz), \quad (69)$$

where μ is the reduced mass and R_{max} is the maximum radiation pressure defined by eq. (46). This equation describes the relative motion of the mirrors driven by the pendulum restoring force and the radiation pressure. A similar equation for the Fabry-Perot cavity with one suspended mirror appeared earlier in refs. [6], [10], [11].

The pendulum restoring force is generated by the usual quadratic potential

$$V_p(x) = \frac{1}{2} \mu \omega_0^2 (z - u)^2, \quad (70)$$

which depends on the control parameter, u . The force due to the radiation pressure is generated by a potential

$$V_{\text{rad}}(z) = -R_{\text{max}} \frac{\arctan[\sqrt{F+1} \tan(kz)]}{k\sqrt{F+1}}, \quad (71)$$

which is derived in the Appendix C.

The sum of the two forces is generated by the effective potential

$$V_{\text{eff}}(z) = V_p(z) + V_{\text{rad}}(z). \quad (72)$$

Thus the relative motion of the mirrors interacting with the electro-magnetic field in the cavity is equivalent to the motion of a particle with the reduced mass in the field of the effective potential. Such representation is valid only in the adiabatic regime, when the delay time can be neglected. Beyond the adiabatic regime the delay time becomes important and the field depends on history of mirror's motion within the storage time.

A remarkable property of the adiabatic regime is that the dynamics is hamiltonian. In other words, we can define a total energy for the motion in the effective potential:

$$\mathcal{E} = \frac{\mu \dot{z}^2}{2} + V_{\text{eff}}(z). \quad (73)$$

Thus the Fabry-Perot cavity in the adiabatic regime is a hamiltonian system. Since there is friction ($\gamma > 0$) the energy is not conserved:

$$\dot{\mathcal{E}} = -\gamma \mu \dot{z}^2 < 0. \quad (74)$$

However, the friction in suspension systems of the gravitational wave detectors is very small. Consequently the energy changes very little (less than a part per million) over a period of the pendulum. Therefore, on time scales of the order of few seconds and even minutes we can think that the energy is conserved.

Note that if there is no friction ($\gamma = 0$) the energy of the motion in the effective potential, eq. (73), is conserved but the combined energy of the mirrors and the electro-magnetic fields in the cavity may not be conserved. The cavity, being multistable, may release or absorb energy as it moves from an unstable to a stable state.

6.3 Global Properties of Effective Potential

The effective potential as a function of cavity length depends essentially on three parameters: F , σ and η . This can be seen if we write the effective potential in terms of dimensionless parameters:

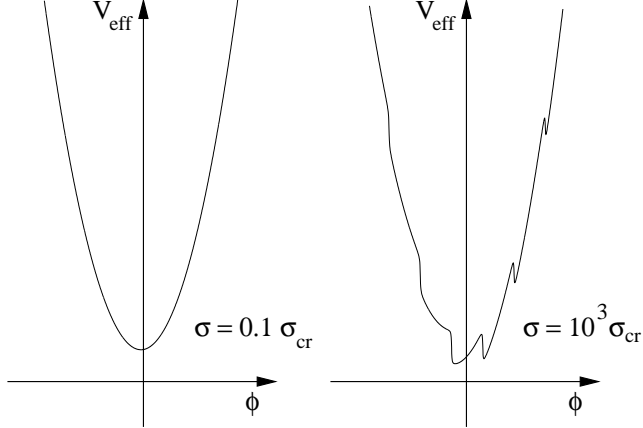
$$V_{\text{eff}} = \frac{\mu \omega_0^2}{k^2} \left[\frac{(\phi - \eta)^2}{2} - \sigma \frac{\arctan(\sqrt{F+1} \tan \phi)}{\sqrt{F+1}} \right]. \quad (75)$$

The overall constant provides correct dimensions to the potential, but otherwise is irrelevant. The parameter σ and the control parameter η can be dynamically adjusted, but the coefficient of finesse, F , cannot be. Therefore, we only consider how the effective potential changes with respect to arbitrary changes in the two parameters: σ and η .

Global properties of the effective potential are defined by one parameter only, σ . For $\sigma < \sigma_{cr}$ the potential has only one minimum and for $\sigma > \sigma_{cr}$ there are several local minima. Effective potential for two different values of σ is shown in Fig. 9. The plots correspond to stable and multistable Fabry-Perot cavities.

The effective potential as a function of two parameters establishes a connection between the dynamics of the Fabry-Perot cavity in the adiabatic regime and the dynamical systems of the catastrophe

Figure 9: Effective potential as function of σ



theory [23]. The catastrophe theory studies singularities (abrupt changes) in equilibrium states of a dynamical system caused by a continuous change of its parameters. The pitchfork bifurcation, as described above, is one of the examples of such singularities.

6.4 Minima and Maxima of the Effective Potential

The control parameter, η , allows us to fine tune the effective potential. By changing the control parameter we can shift the positions of local minima and maxima of the potential. To illustrate this consider the following example. Let the operation point be ϕ_1 as shown in Figure 10.

To make this state an equilibrium we have to adjust the control parameter according the eq. (53). This is equivalent to solving the following equation:

$$\left. \frac{dV_{\text{eff}}}{d\phi} \right|_{\phi=\phi_1} = 0. \quad (76)$$

Since at the point, ϕ_1 , the effective potential has a local minimum:

$$\left. \frac{d^2V_{\text{eff}}}{d\phi^2} \right|_{\phi=\phi_1} > 0 \quad (77)$$

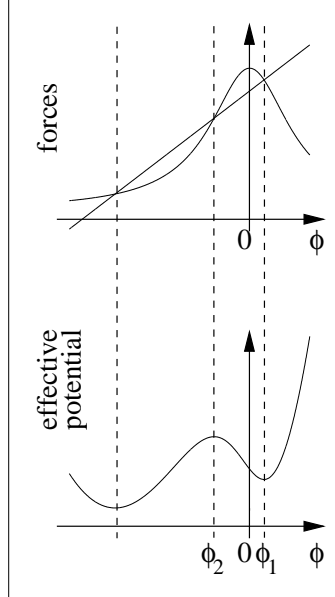
this state is stable. From the figure we see that if we choose the operation point at ϕ_2 , we obtain the same control parameter and arrive at the same effective potential. However, at the point ϕ_2 the effective potential has a local maximum:

$$\left. \frac{d^2V_{\text{eff}}}{d\phi^2} \right|_{\phi=\phi_2} < 0. \quad (78)$$

Therefore, the equilibrium state at ϕ_2 , is unstable.

Thus, stable equilibrium positions correspond to local minima and unstable equilibrium positions correspond to local maxima of the effective potential. By adjusting the control parameter we can turn any state into a stable equilibrium if that state is outside the instability region, eq.(67).

Figure 10: Minimum and maximum of effective potential



7 Resonance of Cavity Length

7.1 Resonant Frequency

A stable equilibrium state of the cavity corresponds to a local minimum of the effective potential. Let the minimum of the effective potential be at z_0 . The small-amplitude mirror motion near this equilibrium state produces harmonic oscillations of the cavity length. The frequency of such oscillations, Ω_0 , is defined by the curvature of the potential at the minimum:

$$\Omega_0^2 = \mu^{-1} \frac{d^2 V_{\text{eff}}}{dz^2} \Big|_{z_0}, \quad (79)$$

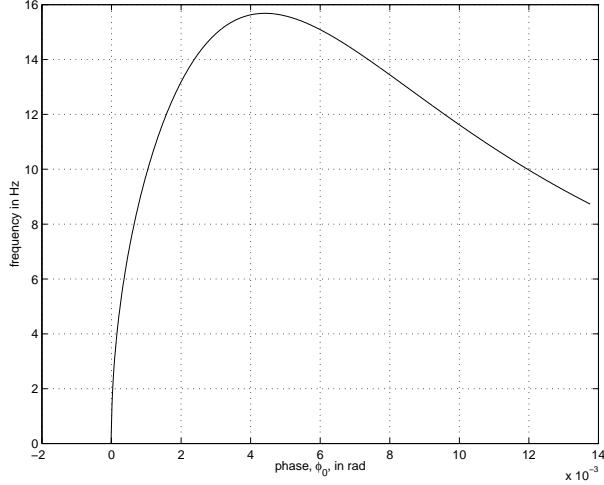
The oscillations of length due to motion of a single mirror, confined in one of the minima of the effective potential were observed by Dorsel et al [6, 7].

Since there are multiple equilibrium states, there are multiple frequencies for the oscillations of the cavity length. Each minimum of the effective potential has its own frequency. These are the resonant frequencies of the cavity length, if the cavity is driven by the external sinusoidal force. At high radiation pressure these frequencies substantially deviate from the pendulum frequency, ω_0 . We find that the frequencies can be expressed entirely in terms of the parameter σ and the location of the minimum:

$$\Omega_0^2(\phi_0) = \omega_0^2 [1 - \sigma A'(\phi_0)], \quad (80)$$

where $\phi_0 = kz_0$ and $A'(\phi_0)$ is the derivative of the Airy function (Appendix C). The plot of $\Omega_0/2\pi$ as a function of the phase ϕ_0 with LIGO parameters is shown in Fig. 11.

Figure 11: Frequency of length oscillations as function of operation point



The frequency reaches maximum at the right inflection point of the Airy profile. The maximum frequency is

$$\Omega_0(\phi_{\text{infl}}) = \omega_0 \left(1 + \frac{\sigma}{\sigma_{cr}}\right)^{\frac{1}{2}}. \quad (81)$$

In LIGO Fabry-Perot cavity the maximum frequency is 15.7 Hz.

7.2 Adjustment of Resonance Frequencies

The resonances of cavity length make the Fabry-Perot cavity a narrow-band transducer between mechanical and optical signals. This observation was made by Dorsel and collaborators [8]. They also suggested that a resonant frequency can be tuned by changing the power of the incident laser. The adjustment of the incident power, which are equivalent to the adjustments of the parameter σ is not the only way to tune the resonant frequency. We can also vary the control parameter. By changing the control parameter we can shift the minimum of the effective potential and thus change the resonant frequency corresponding to that minimum.

On the other hand we may require that the operation point remains fixed as we tune the resonant frequency. This can be done if we vary the two parameters, σ and η , simultaneously so that the equilibrium condition is preserved. For this we need to accompany any change $\delta\sigma$ by the change in the control parameter as follows

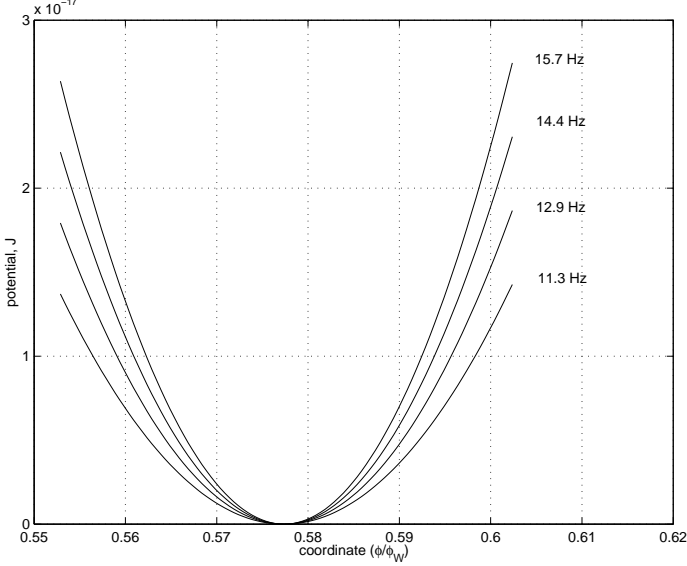
$$\delta\eta = -A(\phi_0) \delta\sigma. \quad (82)$$

This way we change the curvature of the effective potential at the minimum without changing the location of that minimum.

The result is the resonant frequency as a function of the control parameter

$$\Omega_0^2(\eta) = \omega_0^2 \left[1 - (\phi_0 - \eta) \frac{A'(\phi_0)}{A(\phi_0)} \right]. \quad (83)$$

Figure 12: Fine tuning of effective potential



The fine tuning of the effective potential and the corresponding frequencies are shown in Fig. 12.

7.3 Plateaus of the Effective Potential

By tuning the parameters, σ and η , we can make the effective potential more and more flat at one of its minima and even form a plateau:

$$\frac{d^2V_{\text{eff}}}{dz^2} = 0. \quad (84)$$

One way of creating the plateau is to tune the control parameter, η . In this method we flatten the potential by bringing the minimum closer to the nearest local maximum. This method of obtaining the plateau by merging the local minimum with the nearest local maximum has a drawback. Namely, in this method we bring the operation point closer and closer to the instability region, eq. (67).

Another way of forming the plateau at the minimum is to start with lower power ($\sigma < \sigma_{cr}$) and gradually increase the power until the bifurcation occurs ($\sigma = \sigma_{cr}$). In this method we begin with a stable cavity: the effective potential has only one minimum. We have to adjust the control parameter so that the operation point coincides with this minimum:

$$\frac{d^3V_{\text{eff}}}{dz^3} = 0. \quad (85)$$

By increasing the incident power $\sigma \rightarrow \sigma_{cr}$, we make the potential more and more flat at the minimum. At the bifurcation point ($\sigma = \sigma_{cr}$) the plateau is formed.

7.4 Period of Anharmonic Oscillations

The oscillations of length in almost flat potential are anharmonic and can have very large period. At the critical point the potential is of fourth order:

$$V_{\text{eff}}(z) = V_{\text{eff}}(z_0) + \frac{1}{4!} V_{\text{eff}}^{(4)}(z_0)(z - z_0)^4. \quad (86)$$

The period of the anharmonic oscillations in the fourth order potential is

$$T_{\text{osc}} = \Gamma^2 \left(\frac{1}{4} \right) \left[\frac{6\mu}{\pi V_{\text{eff}}^{(4)}(z_0)} \right]^{\frac{1}{2}} \frac{1}{a}, \quad (87)$$

where a is the amplitude of the oscillation. Since the amplitude of mirror motion and correspondingly the amplitude of the length oscillations is very small (of the order of a few μm), the period can be very large.

In practice it is unlikely that the cavity is maintained exactly at the bifurcation point. More likely the long period oscillations are obtained slightly below the critical point $\sigma < \sigma_{cr}$. In this case the potential is not quartic, nonetheless the oscillations have long period, which can be found from a general expression

$$T_{\text{osc}} = \sqrt{2\mu} \int_{z_1}^{z_2} \frac{dz}{[\mathcal{E} - V_{\text{eff}}(z)]^{\frac{1}{2}}}, \quad (88)$$

where z_1 and z_2 are the turning points of the oscillations. Both equations (87) and (88), appear in books on Mechanics, for example in ref. [24].

In Table 2 we show numerical values of frequencies of the oscillations in the nearly flat potential for LIGO Fabry-Perot cavities. The flatness of the potential is characterized by the deviation of the parameter σ from its critical value. The table shows that we can achieve period substantially greater

Table 2: Period of anharmonic oscillations in almost flat potential

amplitude (m)	period (s)			
	a	$\sigma = 0.96 \sigma_{cr}$	$\sigma = 0.98 \sigma_{cr}$	$\sigma = \sigma_{cr}$
10^{-8}		1.34	1.34	1.33
10^{-9}		2.31	2.36	2.41
10^{-10}		6.39	8.74	23.2
10^{-11}		6.68	9.44	234.2

than the pendulum period ($2\pi/\omega_0 \approx 1.3$ s). This method of obtaining very long period by taking advantage of the radiation pressure is an interesting alternative to the very long suspension.

8 Implications for Control System

8.1 Pound-Drever Locking Servo

The operation point of the cavity is a stable equilibrium length which corresponds to a minimum of the effective potential. Due to the ambient seismic motion the actual state of the cavity is constantly moving near the operation point. Often the minimum of the effective potential is not deep enough to confine the state. In such case a negative feedback control system (servo) is used to keep the cavity state within the minimum. The dynamics of the cavity with the control system is described by the same equations as before but the control parameter, u , becomes a function of the cavity length. In LIGO interferometers the control function, $u(z)$, is proportional to the Pound-Drever signal, eq. (11):

$$u(z) \propto \text{Im}\{E(t)\}. \quad (89)$$

Such control function depends on the cavity length z and does not depend on the cavity center of mass.

There is no explicit analytic expression for the function $u(z)$, given by eq. (89), which is valid for all dynamical regimes. However, in the adiabatic regime we can obtain a simple formula

$$u(z) = -\left(\frac{G}{2k}\right) \frac{\sin 2kz}{1 + F \sin^2 kz} + u_0, \quad (90)$$

where G is the gain and u_0 is the dc-bias of the control system. The minus sign in eq. (90) accounts for the negative feedback.

If the deviation of the cavity length from the nearest fringe is much less than the width of the resonance the control signal becomes linear:

$$u(z) \approx -G \left(z - n \frac{\lambda}{2}\right) + u_0, \quad (91)$$

where n is the order of the fringe. Since the amplitude of motion of the mirrors is small (of the order of a micron) the fringe order number is a small number: $n = 0, \pm 1, \pm 2, \dots$.

8.2 Multistability in Presence of Servo

Since the control law eq. (90) is a periodic function of the cavity length the cavity with the servo is multistable. To study multistability in dynamics of the cavity with the control system we introduce the static servo potential

$$V_{\text{svo}}(z) \equiv -\mu\omega_0^2 \int_0^z u(z') dz' \quad (92)$$

$$\propto \ln(1 + F \sin^2 kz). \quad (93)$$

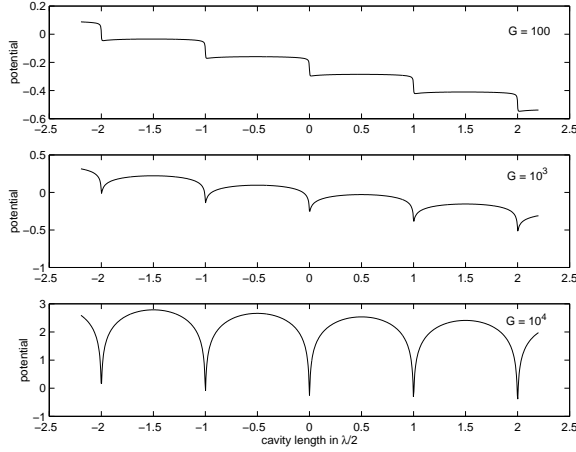
Therefore, in the adiabatic regime the dynamics of the cavity with the servo can be described by the combined potential

$$V_{\text{eff}} + V_{\text{svo}} = \frac{\mu\omega_0^2}{k^2} \left[\frac{(\phi - \eta)^2}{2} - \sigma \frac{\arctan(\sqrt{F+1} \tan \phi)}{\sqrt{F+1}} - \frac{G}{2F} \ln A(\phi) \right], \quad (94)$$

where the dc-bias is conveniently assigned to the pendulum potential ($\eta = ku_0$).

For large-amplitude mirror motion the control function, $u(z)$, is nonlinear and, therefore, the servo acts as a nonlinear device. The effect of the servo depends on the gain, G , and can be made stronger than the effect of the radiation pressure. Fig. 13 shows the sum of the radiation pressure potential and the servo potential for three different values of the servo gain: $G = 10^2, 10^3, 10^4$. On the first plot

Figure 13: Combined radiation pressure and servo potential



the sum of the two potentials looks like a staircase which is characteristic of the radiation pressure potential. Here the effect of the servo is negligible compared to the effect of the radiation pressure. On the second plot the “staircase” shows dips created by the servo. Here the effect of the servo is comparable to the effect of radiation pressure. On the third plot the dips are bigger than the steps, and the servo dominates the radiation pressure.

8.3 Equilibrium and DC-bias

Stable equilibrium states of the cavity with the servo are the minima of the combined potential:

$$\frac{d}{dz}(V_{\text{eff}} + V_{\text{servo}}) = 0. \quad (95)$$

This condition can also be seen as a requirement on the dc-bias. Namely, a cavity state, z_0 , becomes an equilibrium if the dc-bias is set according to the equation:

$$u_0 = z_0 - \frac{\sigma}{k} \left(1 - \frac{G}{2\sigma} \sin 2kz_0 \right) A(kz_0). \quad (96)$$

From this equation we see that, in general, the dc-bias is connected to the gain of the servo. Therefore, changes of the servo gain should be accompanied by the corresponding changes of the dc-bias. Otherwise the equilibrium condition will be lost and the equilibrium state will change. There is one exception to this rule. In the case when the operation point is chosen at the peak of the Airy function

$(z_0 = \frac{\lambda}{2})$ the dc-bias becomes independent of the gain:

$$u_0 = n \frac{\lambda}{2} - \frac{\sigma}{k}. \quad (97)$$

Note the dependence of the dc-bias on the fringe number, n .

8.4 Stability Provided by Servo

The negative feedback control system can turn an unstable state of the cavity into a stable one. It can also provide greater stability margins to the already stable cavity. These effects of the servo can be analyzed with the help of the servo potential.

The frequency of the cavity length oscillations in the presence of the servo is

$$\Omega_0^2 \equiv \mu^{-1} \frac{d^2}{dz^2} (V_{\text{eff}} + V_{\text{svo}}) \quad (98)$$

$$= \omega_0^2 \left\{ 1 - \sigma A'(\phi_0) + G[1 - (F + 2) \sin^2 \phi_0] A^2(\phi_0) \right\}, \quad (99)$$

By adjusting the gain we can vary this frequency in a wide range. We can also turn the unstable state ($\Omega_0^2 < 0$) into a stable one ($\Omega_0^2 > 0$). In particular we can make stable any state of the cavity within a width of the fringe ($|\phi_0| < \phi_w$). This can be done by choosing a sufficiently high servo gain. For LIGO parameters such gain is $G \approx 1800$.

9 Conclusions

The suspended mirrors in the Fabry-Perot cavity are described as a pair of harmonic oscillators driven by nonlinear forces of the radiation pressure. The oscillators are not independent; they interact with each other through the laser circulating in the cavity. The normal coordinates for the coupled oscillators are the position of their center of mass and the cavity length, both affected by the delay in the cavity. The radiation pressure has almost no effect on the motion of the center of mass, but affects strongly the dynamics of the cavity length. To understand universal properties of the Fabry-Perot cavity as a nonlinear dynamical system we introduced two parameters. These parameters determine qualitative behavior of the dynamics of the cavity length common to all Fabry-Perot cavities with suspended mirrors. The first parameter determines whether the cavity is multistable or not. There is a critical value for this parameter, at which the bifurcation occurs, and the cavity becomes multistable. The second parameter is the generalized control force. It determines the locations of the equilibrium states. If the control parameter varies within a wide range the equilibrium state of the cavity follows a hysteresis loop. We analyze stability of the equilibrium states and identify the instability region. The instability is explained in terms of the effective potential: stable states correspond to local minima of the effective potential and unstable states correspond to local maxima. Each minimum of the effective potential defines the resonance frequencies of the cavity length oscillations. These resonances make the cavity a narrow band detector of any disturbances which affect the optical path of the laser in the cavity, such as mechanical vibrations of the mirrors. The resonance frequencies can be tuned by changing both of the parameters.

The nonlinear dynamics, described in this paper, provides grounds for building a control system for the Fabry-Perot cavities in the interferometric gravitational detectors. Our results can also be used in the studies of the Fabry-Perot cavities near the quantum limit.

References

- [1] C. Bradaschia, R. Delfabbro, A. Divirgilio, A. Giazotto, H. Kautzky, V. Montelatici, D. Pasuello, A. Brillet, and O. Cregut et al. Terrestrial gravitational noise on a gravitational wave antenna. *Nuclear Instruments A*, 289:518, 1990.
- [2] A. Abramovici, W.E. Althouse, R.W. Drever, Y. Gursel, S. Kawamura, F.J. Raab, D. Shoemaker, L. Sievers, R.E. Spero, K. Thorne, R.E. Vogt, R. Weiss, S.E. Whitcomb, and E. Zucker. LIGO: The Laser Interferometer Gravitational-wave Observatory. *Science*, 256:281–412, April 17 1992.
- [3] K. Tsubono. 300-m laser interferometer gravitational wave detector (TAMA 300) in Japan. In *Proceedings of First Eduardo Amaldi conference on gravitational wave experiments, Frascati, Roma, June 1994*, pages 112–114, Singapore, 1995. World Scientific.
- [4] N. Minorsky. *Nonlinear Oscillations*. D. Van Nostrand Company, Inc., 1962.
- [5] V.B. Braginskii and A.B. Manukin. *Measurement of weak forces in physics experiments*. University of Chicago Press, 1977.
- [6] A. Dorsel et al. Optical bistability and mirror confinement induced by radiation pressure. *Physical Review Letters*, 51(17):1550–1553, October 1983.
- [7] A. Dorsel et al. Optical resonators driven by radiation pressure. *Philosophical Transactions of the Royal Society of London A*, 313:341–347, 1984.
- [8] A. Dorsel et al. Light-pressure mirror stabilization. *Acta Physica Austriaca*, 57:133–138, 1985.
- [9] P. Meystre et al. Theory of radiation-pressure-driven interferometers. *Journal of the Optical Society of America B*, 2(11):1830–1839, November 1985.
- [10] N. Deruelle and P. Tourrenc. The problem of the optical stability of a pendular Fabry-Perot. In *Gravitation, Geometry and Relativistic Physics*, pages 232–237, Berlin, 1984. Springer-Verlag.
- [11] Ph. Tourrenc and N. Deruelle. Effects of the time delays in a non linear pendular Fabry-Perot. *Annales de Physique*, 10:241–252, June 1985.
- [12] J. Aguirregabiria et al. Delay-induced instability in a pendular Fabry-Perot cavity. *Physical Review A*, 36(8):3768–3770, October 15 1987.
- [13] L. Bel et al. Pendular Fabry-Perot cavities as a paradigm for the dynamics of system with delays. *Physical Review A*, 37(5):1563–1570, March 1988.
- [14] B. Meers and N. MacDonald. Potential radiation-pressure-induced instabilities in cavity interferometers. *Physical Review A*, 40(7):3754–3763, October 1989.

- [15] V. Chickarmane, S.V. Dhurandhar, R. Barellet, P. Hello, and J.-Y. Vinet. Radiation pressure and stability of interferometric gravitational-wave detectors. *Applied Optics*, 37(15):3236–3245, May 1998.
- [16] M. Rakhmanov. Dynamics of Fabry-Perot resonators with suspended mirrors. 2. Delay effects and control system. LIGO technical report T970230, California Institute of Technology, February 1998.
- [17] M. Born and E. Wolf. *Principles of Optics*. Pergamon Press, Oxford, 6 edition, 1980.
- [18] J.H. Marburger and F.S. Felber. Theory of a lossless nonlinear Fabry-Perot interferometer. *Physical Review A*, 17(1):335–342, January 1978.
- [19] G. Rowlands. *Non-linear phenomena in science and engineering*. Ellis Horwood, 1990.
- [20] A.A. Andronov, A.A. Vitt, and S.E. Khaikin. *Theory of Oscillators*. Pergamon Press, Oxford, New York, 1966.
- [21] H.M. Gibbs. *Optical Bistability: Controlling Light with Light*. Academic Press, Inc., Orlando, Florida, 1985.
- [22] B.S. Wherrett and S.D. Smith F.R.S, editors. *Optical Bistability, Dynamical Nonlinearity and Photonic Logic*, London, 1985. A Royal Society Discussion Meeting held on 21 and 22 March 1984, organized by S.D. Smith, F.R.S, A. Miller and B.S. Wherrett, The Royal Society.
- [23] V.I. Arnold. *Catastrophe theory*. Springer-Verlag, Berlin, New York, 1984.
- [24] L.D. Landau and E.M. Lifshitz. *Mechanics*. Pergamon Press, Oxford, New York, 3 edition, 1989.

A Parameters of LIGO Fabry-Perot Cavities

The following table shows the transmissivities and the losses for the 40m and 4 km LIGO mirrors.

Table 3: Transmissivity and reflectivity of LIGO mirrors

Mirror #	parameter	40m Prototype	4km LIGO
input mirror	t_a	0.0758	0.1732
	r_a	0.9971	0.9849
end mirror	t_b	0.0035	0.0045
	r_b	0.999944	0.999965

Other parameters for LIGO cavities are listed in the following table

Table 4: Parameters of 40m and 4km LIGO cavities

Parameter (units)	Symbol	40m Prototype	4km LIGO
laser wavelength (m)	λ	5.14×10^{-7}	1.06×10^{-6}
cavity length (m)	L_0	38.5	4000
delay time (s)	T	1.28×10^{-7}	1.33×10^{-5}
storage time (s)	τ	8.60×10^{-5}	1.74×10^{-3}
free spectral range (Hz)	f_{FSR}	3.89×10^6	3.75×10^4
cavity low-pass freq. (Hz)	f_{cav}	1.85×10^3	91.2
cavity gain	G_{cav}	645	130
coefficient of finesse	F	4.47×10^5	1.71×10^4
phase width (rad)	ϕ_w	1.49×10^{-3}	7.64×10^{-3}
displacement width (m)	x_w	1.22×10^{-10}	1.29×10^{-9}
Finesse	Finesse	1051	205
mirror mass (kg)	m_a	1.53	10.8
pendulum frequency (Hz)	$\omega_0/2\pi$	1.0	0.77

B Derivation of Field Equations

We approximate the laser by a plane electro-magnetic wave with electric field, $f(x, t)$, which is a solution of the 1-dimensional wave equation:

$$\frac{1}{c^2} \frac{\partial^2 f}{\partial t^2} - \frac{\partial^2 f}{\partial x^2} = 0. \quad (100)$$

Let $f_1(x, t)$ be the electric field corresponding to the right-moving wave in the cavity and $f_2(x, t)$ be the electric field corresponding to the left-moving wave. We define the complex amplitudes at the reference planes, located at $x = 0$ and $x = L_0$. The amplitudes of the right-moving wave, E_1 and E'_1 , are defined by the following equations:

$$f_1(0, t) = E_1(t)e^{i\omega t}, \quad (101)$$

$$f_1(L_0, t) = E'_1(t)e^{i\omega t}. \quad (102)$$

Similarly, we define the amplitudes, E_2 and E'_2 , for the left-moving wave:

$$f_2(0, t) = E'_2(t)e^{i\omega t}, \quad (103)$$

$$f_2(L_0, t) = E_2(t)e^{i\omega t}. \quad (104)$$

Since the wave functions satisfy the wave equation their values at different locations can be obtained by delay:

$$f_1(L_0, t) = f_1(0, t - L_0/c), \quad (105)$$

$$f_2(0, t) = f_2(L_0, t - L_0/c). \quad (106)$$

Therefore, the amplitudes at the two reference planes are related to each other:

$$E'_1(t) = E_1(t - L_0/c)e^{-ikL_0}, \quad (107)$$

$$E'_2(t) = E_2(t - L_0/c)e^{-ikL_0}. \quad (108)$$

If we assume that

$$L_0 = N \frac{\lambda}{2}, \quad (109)$$

where N is an integer, we obtain the equations (3-4).

The equation for the reflection off the end mirror can be obtained from the condition of continuity of the wave function at the mirror surface:

$$f_2(L_0 + x_b, t) = -r_b f_1(L_0 + x_b, t). \quad (110)$$

Therefore, at the reference plane $x = L_0$:

$$f_2(L_0, t + x_b/c) = -r_b f_1(L_0, t - x_b/c). \quad (111)$$

This equation can now be written in terms of the amplitudes:

$$E_2(t + x_b/c) = -r_b E'_1(t - x_b/c)e^{-2ikx_b}. \quad (112)$$

If we neglect the small time delay due to the mirror motion, x_b/c , we obtain the equation (5). Other equations can be derived similarly.

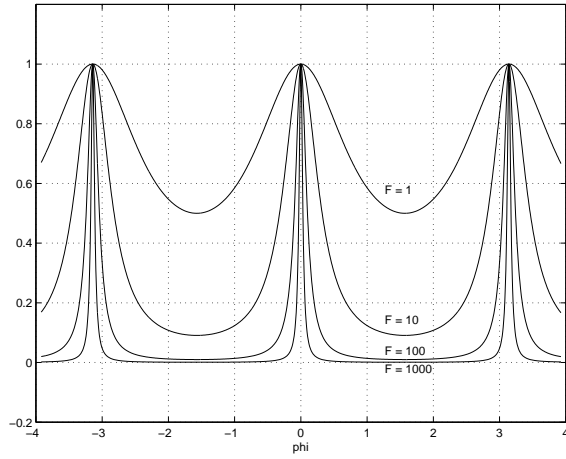
C Some properties of Airy function

Here we present few basic properties Airy function, which are used throughout this paper. The Airy function,

$$A(\phi) = \frac{1}{1 + F \sin^2 \phi}, \quad (113)$$

is a positive, periodic function of ϕ with the period π . The Airy function depends on one parameter, F , a positive number called the coefficient of finesse. Fig. 14 shows Airy functions with different coefficients of finesse.

Figure 14: Airy Profile



The half-width, ϕ_w , is the phase, at which the Airy function equals to half of its maximum value

$$\phi_w \equiv \arcsin \frac{1}{\sqrt{F+2}} \approx \frac{1}{\sqrt{F}}. \quad (114)$$

The full width is equal to $2\phi_w$. Finesse is the ratio of the separation between the peaks to the full width of the peak

$$\text{Finesse} \equiv \frac{\pi}{2\phi_w} \approx \frac{\pi}{2}\sqrt{F}. \quad (115)$$

A slope of a tangent line to Airy function at point ϕ is defined by the derivative of Airy function

$$A'(\phi) = -\frac{F \sin 2\phi}{(1 + F \sin^2 \phi)^2}. \quad (116)$$

The inflection points of Airy function can be found by solving the equation: $A''(\phi) = 0$. They are located at $\pm\phi_{\text{inf}}$, where

$$\cos 2\phi_{\text{inf}} = \frac{1}{2F} \left(\sqrt{9F^2 + 4F + 4} - F - 2 \right). \quad (117)$$

The greatest slope the tangent line achieves at the left inflection point $\phi = -\phi_{\text{inf}}$. This maximum slope is

$$A'(-\phi_{\text{inf}}) = \frac{\left[\frac{1}{2}(F+2)\sqrt{9F^2+4F+4} - \frac{3}{2}F^2 - 2F - 2\right]^{1/2}}{\left(\frac{1}{4}\sqrt{9F^2+4F+4} - \frac{3}{4}F - \frac{3}{2}\right)^2}. \quad (118)$$

The expression for the inflection points, eq. (117), and the maximum slope, eq. (118), are quite complicated, therefore, it is useful to find simple approximate formulas for these quantities. For high finesse cavities (large F - limit) such approximations can be easily found:

$$\phi_{\text{inf}} \approx \frac{1}{\sqrt{3F}}, \quad (119)$$

$$A'(-\phi_{\text{inf}}) \approx \frac{3}{8}\sqrt{3F}. \quad (120)$$

Any straight line, which has a slope greater than the maximum slope, intersects the Airy function at only one point. If the slope of the line is less than the maximum slope the line can intersect the Airy function at more than one point.

The integral of Airy function can be found in terms of elementary functions

$$\int_0^\phi A(\phi')d\phi' = \frac{\arctan(\sqrt{F+1}\tan\phi)}{\sqrt{F+1}}. \quad (121)$$

This expression is used in defining the potential for the radiation pressure in the adiabatic approximation.